Thin NaCl films on silver (001): island growth and work function

Gregory Cabailh, Claude R Henry, Clemens Barth

Thin NaCl films on silver (001): island growth and work function

2012 New J. Phys. 14 103037

(http://iopscience.iop.org/1367-2630/14/10/103037)

New Journal of Physics
The open-access journal for physics

Thin NaCl films on silver (001): island growth and work function

Gregory Cabailh[1], **Claude R Henry and Clemens Barth**[1]
Aix Marseille University, CNRS, CINaM UMR 7325,
F-13288 Marseille Cedex 09, France
E-mail: cabailh@insp.jussieu.fr and barth@cinam.univ-mrs.fr

New Journal of Physics **14** (2012) 103037 (18pp)
Received 27 July 2012
Published 23 October 2012
Online at http://www.njp.org/
doi:10.1088/1367-2630/14/10/103037

Abstract. The surface work function (WF) and substrate temperature dependence of the NaCl thin-film growth on Ag(001) have been studied by noncontact atomic force microscopy and Kelvin probe force microscopy. In the sub-monolayer range, the NaCl film is composed of large crystalline islands, which decrease in density and increase in size with increasing temperature during deposition. Each island is composed of a large base island 2 monolayers (ML) thick (for $T > 343$ K), which collects impinging NaCl molecules that form ad-islands on top. Kelvin probe force microscopy (KPFM) measurements show a reduction of the silver WF by $\Delta\varphi = \varphi_{Ag} - \varphi_{NaCl/Ag} = 0.69 \pm 0.03$ eV with no dependence on the film thickness (1–6 ML), in agreement with recent theoretical calculations. The previously observed nanometer-sized moiré pattern on islands that are 45° rotated with respect to the silver lattice could be observed in the scanning tunneling microscopy mode. However, no contrast could be obtained in KPFM images.

[1] Authors to whom any correspondence should be addressed.

Contents

1. Introduction

Thin ionic films grown on metal surfaces have become very important interfaces in many scientific disciplines as shown for magnesium oxide films in microelectronics [1, 2] and catalysis [3, 4]. Alkali halide thin films, on the other hand, are used for supporting single atoms and molecules such that the intrinsic electronic properties of these nano-objects are partially decoupled from the conducting metal support [5–8, 12–15]. A dramatic increase over the last few years of publications dealing with alkali halide films was observed, in particular because such films can be grown at relatively low temperatures on almost any conducting surface exhibiting large crystalline, defect-free and atomically flat terraces—a requisite for self-assembly [5–7], conduction [8], friction [9], atomic resolution imaging of molecules [10, 11] and manipulation experiments [12–16]. Interestingly, these thin films is that they can be nanotemplated on vicinal surfaces [17, 18] and even manipulated [19].

An important characteristic of ionic thin films on metal surfaces is that the work function (WF) of the surface is substantially lowered by the film [20–24]. This is of importance in catalysis, for instance, where under specific circumstances a charge transfer from the metal substrate to supported metal clusters can change the catalytic properties of the clusters [25]. Furthermore, it has been stated that depending on the thin-film epitaxy [26] the WF can vary laterally on the film [22, 23, 27, 28] but may also change with varying thickness [24, 29], both having a high impact on supported molecules and clusters [30].

For characterizing the film morphology and supported nano-objects, scanning tunneling microscopy (STM) can be used since ionic films are mostly prepared such that they are only a few atomic layers thick. Local surface WF measurements can be made indirectly by using STM spectroscopy [22, 23, 27]. However, a much more direct way is to *image* surface WF changes by using noncontact atomic force microscopy (nc-AFM) and Kelvin probe force microscopy (KPFM) [29, 31–33]. While imaging the surface topography in the nc-AFM mode, a second image is obtained simultaneously, which directly represents surface WF changes with mV resolution and a lateral resolution at the nanometer scale [34, 35]. In particular, the combination

of nc-AFM and KPFM has great potential for studying thin-film systems and supported nano-objects [36].

To obtain high-quality alkali halide thin films and to control the properties of such films on metal surfaces (lateral size, island thickness, etc), the detailed film growth needs to be understood, especially as a function of growth parameters such as substrate temperature, coverage and incoming flux. This has recently been done by spot-profile-analysis low-energy electron diffraction (SPA-LEED) [37]. To complete the picture, local information at the nanometer scale is needed, which can be done by scanning probe microscopy such as nc-AFM. Furthermore, to well characterize the WF change of the metal surface by the film, a systematic analysis from the KPFM point of view is required. This helps to quantify possible lateral variations and the thickness dependence of the surface WF. We address all these aspects and concentrate on NaCl(001) thin films on the silver (001) surface—a commonly used thin-film system in surface science [7, 22–24, 37–40].

2. Experimental methods

Noncontact AFM and KPFM experiments were performed in an ultra-high vacuum (UHV) chamber (low 10^{-10} mbar base pressure) [41] with an Omicron room temperature AFM/STM (digital demodulator from NanoSurf). Conducting silicon cantilevers with resonance frequencies of 70 kHz or 300 kHz (NANOSENSORS PPP-QFMR (75 kHz) PPP-QNCHR (300 kHz), p-Si, 0.015 Ω cm) were used, whose peak-to-peak amplitudes A were kept constant during the imaging. For the frequency-modulated KPFM measurements [35], the tip is grounded and a dc (U_{dc}) and an ac voltage (U_{ac}) with frequency f_{ac} are applied on the sample [42]. The Kelvin modulation is applied during the normal topography imaging so that a topography and a Kelvin image are simultaneously obtained. At each spot on the surface, the contact potential difference between the tip and the surface U_{CPD} is measured (Kelvin voltage), and the contrast in Kelvin images represents variations of the surface WF. Images were acquired with an Omicron SCALA system and analyzed with Gwyddion software[2].

Ag(001) substrates were prepared by cycles of Ar^+ sputtering ($E = 1.5$ keV) and annealing to 773 K. NaCl thin films were then grown onto the Ag substrate held at various temperatures (306–483 K) using a homemade Knudsen cell, by heating to sublimation an NaCl crystal at 830 ± 20 K placed in a closed alumina crucible with a flux of 0.025 MLE min^{-1} (0.007 nm min^{-1} or 2.6×10^{11} NaCl molecules $s^{-1}cm^{-2}$). One monolayer equivalent (MLE) is defined as one NaCl crystallographic plane, whose height is half the unit cell in the [001] direction, 0.282 nm ($a_{NaCl} = 0.564$ nm [43]). Heights were calibrated using monoatomic high silver steps, 0.204 nm ($a_{Ag} = 0.407$ nm [44]).

3. Film growth

During the growth of NaCl thin films, the Ag substrate was held at various temperatures (T_{Ag}) ranging from room temperature (RT) up to 483 K. Noncontact AFM and KPFM measurements for five specific deposition temperatures (306, 343, 373, 423 and 443 K) with all other parameters kept constant are depicted in figure 1. The characteristics of the thin films are summarized in table 1. Note that for each temperature, the silver surface was cleaned and a new film was prepared.

[2] http://gwyddion.net/ (2012).

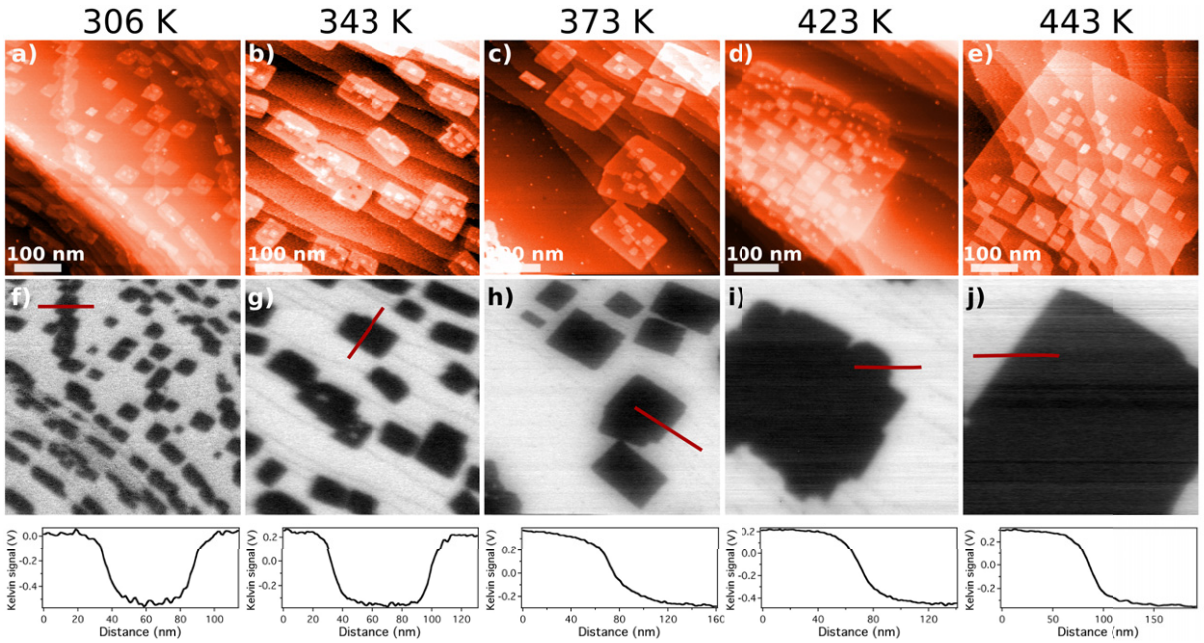

Figure 1. nc-AFM (top) and KPFM (bottom) images of 0.75 MLE thin NaCl films grown on Ag(001) held at various temperatures as indicated above each column. Each film was separately grown after cleaning the Ag(001) substrate by sputtering and annealing. The line profiles of the Kelvin images were taken over the edges of the islands and represent the WF change between Ag(001) and NaCl/Ag(001). Imaging parameters: $500 \times 500\,\mathrm{nm}^2$, speed $= 0.5$ Hz, $A = 22$ nm, $f_{\mathrm{ac}} = 474$ Hz, $U_{\mathrm{ac}} = 150$ mV (d, i: 250 mV and e, j: 100 mV). Δf (Hz) $= -19$ (a), (c), (f), (h); -8 (b), (g); -49 (d), (i); and -17 (e), (j).

3.1. Island size, density and orientation

For $T_{\mathrm{Ag}} = \mathrm{RT}$ (figure 1(a)), the islands have a rectangular shape and are mostly pinned at the Ag step edges, which act as nucleation sites for the first layer. However, islands can also be found on terraces if these are sufficiently large (>100 nm). The islands have an equivalent edge length of 36 nm assuming a square shape and a density of 2.3×10^{10} islands cm^{-2} with a height that corresponds to one or two NaCl atomic layers. We stress here that we observed 1 monolayer (ML) thick islands ($h = a_{\mathrm{NaCl}}/2 = 0.28$ nm) mostly at $T_{\mathrm{Ag}} = \mathrm{RT}$. An example of these 1 ML islands is shown in figure 2(a) with the corresponding profiles (figure 2(c)). The edges of this island are 0.46 nm high, indicative of 2 ML high NaCl, whereas the inner part of the island is only 0.24 nm high, corresponding to a single monolayer. Interesting to note is that the formation of the second layer takes place at the edges of the island (bright rim) leaving the center of the island still 1 ML thick. From analyzing many images, we also noticed that once the second layer has grown and completed, the islands have a higher degree of order expressed by a more symmetric island shape (compare islands 1 and 2).

When the temperature is increased from RT to $T_{\mathrm{Ag}} = 343$, 373, 423 and 443 K (figures 1(b)–(e)), the island size increases by a factor of 3.6, 5.8, 63 and 123, whereas the density decreases by 3.1, 6.6, 59 and 110. As at RT, the islands are pinned at Ag steps and

Table 1. Properties of the NaCl thin films grown at different substrate temperatures T_{Ag} at a constant nominal thickness of 0.75 MLE. The parameters A_{base}, a, ρ, C, $KPFM_h$ and $KPFM_p$ denote the average experimental size of the base islands (A_{base} in 10^{-11} cm^2), the side length in nm of the island assuming a square shape ($a = b$), the island density ($\times 10^8$ islands cm^{-2}), the percentage of Ag(001) surface covered by NaCl islands (%) and the Kelvin signal (meV) measured using a histogram (h) or a line profile (p).

T_{Ag}	306 K	343 K	373 K	423 K	443 K
A_{base}	1.3 ± 0.1	4.7 ± 0.3	7.5 ± 1.0	82 ± 10	160 ± 24
$a = b$	36	69	87	286	400
ρ	230 ± 20	74 ± 2	35 ± 2	3.9 ± 0.3	2.1 ± 0.2
C	29 ± 2	35 ± 2	28 ± 2	32 ± 2	34 ± 2
$A \times \rho$	0.299	0.348	0.210	0.262	0.336
$KPFM_h$	428 ± 8	618 ± 8	501 ± 30	691 ± 13	693 ± 6
$KPFM_p$	504 ± 20	675 ± 15	681 ± 20	690 ± 20	710 ± 20

expand on the upper and lower Ag terraces, indicating a strong inter-step diffusion. Films that are prepared at the highest temperature of 443 K exhibit very large islands with an average edge length of up to 400 nm, which strongly contrasts with MgO films on the same substrate [45]. Very important to mention is that, starting from $T_{Ag} = 373$ K, all the islands have a base layer 2 ML thick (*base islands*). All successive third and fourth layers (*ad-islands*) on top of the 2 ML base islands are often pinned on the underlying Ag step, as observed by Pivetta *et al* [22]. The ad-islands have a height that always corresponds to 1 ML. A striking difference with respect to the growth of the second layer is that the ad-islands are located somewhere on the top but never at the edges of the base layer (figures 1(c)–(e) and 2(e)). Note that for $T_{Ag} = 483$ K, no NaCl could be observed to adsorb on the Ag(001) surface.

With the statistical values from table 1, the island density is plotted as a function of T_{Ag} (figure 2(g)). The density decreases monotonically with increasing temperature and two branches can be clearly observed. Each branch depends exponentially on the temperature in the form of $\rho = \rho_0 \times \exp(-\frac{\Delta E}{k_B T_{Ag}})$, where ρ is the island density, k_B the Boltzmann constant and ρ_0 a constant. The energies deduced from the fits are $\Delta E_1 = 0.30$ eV (306–373 K) and $\Delta E_2 = 0.66$ eV (413–443 K).

To determine the exact crystalline orientation of the islands with respect to the Ag lattice, we imaged the Ag(001) surface and the NaCl islands with atomic resolution (see figures 2(e_1) and (e_2)). The majority of NaCl islands are orientated in the main crystallographic direction of Ag with their [001] directions parallel ($[001]_{Ag} \parallel [001]_{NaCl}$); they are often referred to as 0° NaCl islands. A second type of island is rotated by 45° with respect to the Ag lattice such that $[001]_{NaCl} \parallel [011]_{Ag}$ [22, 37] (45° *NaCl islands*). Pivetta *et al* [22] observed the latter islands only at step edges; in very few cases we do observe them on terraces. Some islands are slightly off axis from both rotations, with a difference in rotation of up to 15°, which can be best seen in LEED images (figure 2(f)): the outer symmetric spots (1) correspond to the Ag ⟨10⟩ spots, whereas the azimuthal elongated spots (2) correspond to the slight deviations in rotation of the NaCl islands, which is in agreement with previous SPA-LEED measurements [37, 39].

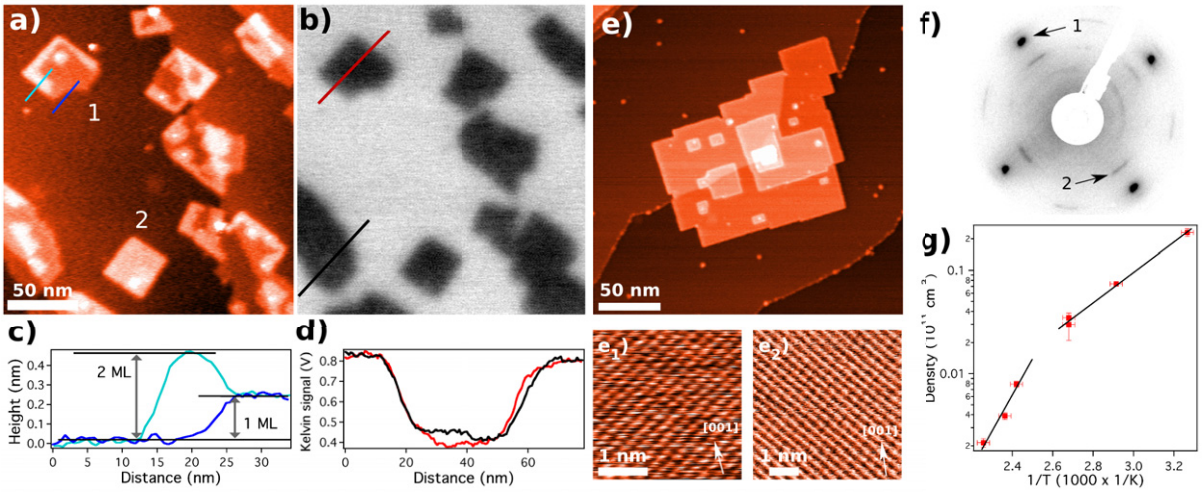

Figure 2. (a) nc-AFM image of a NaCl thin film grown on Ag(001) at 306 K during deposition. (b) Corresponding KPFM image. (c, d) Line profiles taken over the island edges in (a) and (b), respectively. Because of the small island sizes the tip–surface convolution reduced the regular WF change from 700 mV down to ∼450 mV (d). (e) A well-defined NaCl island grown at 423 K and atomic resolution obtained on Ag(001) and on a NaCl island. (f) LEED measurement of NaCl/Ag(001) grown at 443 K recorded at $E = 55.3$ eV. The darker spots (1) correspond to Ag(001), whereas spots (2) correspond to the NaCl films. (g) Island density in the logarithmic scale as a function of the reciprocal temperature T_{Ag} ($T_{Ag} = 306$, 343, 373, 413, 423 and 443 K). Imaging parameters: (a), (b) $187 \times 198\,nm^2$, speed = 0.5 Hz, $A = 22$ nm, $f_{ac} = 483$ Hz, $U_{ac} = 150$ mV, $\Delta f = -31$ Hz, (e) $250 \times 250\,nm^2$, speed = 0.5 Hz, $A = 15$ nm, $f_{ac} = 474$ Hz, $U_{ac} = 250$ mV, $\Delta f = -8$ Hz, (e_1) STM, $U_{bias} = 1$ V, $I = 3$ nA, $3.75 \times 3.75\,nm^2$, speed = 3 Hz, (e_2) nc-AFM, $\Delta f = -70$ Hz, $6.25 \times 6.25\,nm^2$, speed = 10 Hz.

3.2. Growth as a function of NaCl quantity

A very important aspect in the growth of thin NaCl films on metal surfaces is the development of the film morphology with respect to the quantity of NaCl that is deposited—understanding and control of this is a requisite for preparing thick, well-defined insulating films. Figure 3 presents a comparison of two different coverages (0.75 and 1.5 MLE) of NaCl deposited at $T_{Ag} = 306$ and 373 K and table 2 summarizes all the properties of the films.

The topography images clearly describe what happens when the amount of NaCl deposited is increased: at RT ($T_{Ag} = 306$ K), the average island size increases by a factor of 1.3 when the amount of NaCl is doubled (from 0.75 to 1.5 MLE), whereas for the island density only a slight increase can be observed (×1.09)—the deposited NaCl is obviously used to build the 2 ML base islands. A different situation can be found at the higher temperature of $T_{Ag} = 373$ K: we observe that the average size of the base islands increases almost fourfold (×3.7) but at the same time the island density almost halves (×0.46)—a signature of an increase of the island size by the incoming NaCl but also by a partial coalescence of the islands. For both temperatures the product of the density times the island size ($A \times \rho$) increases equally by a factor of 1.5.

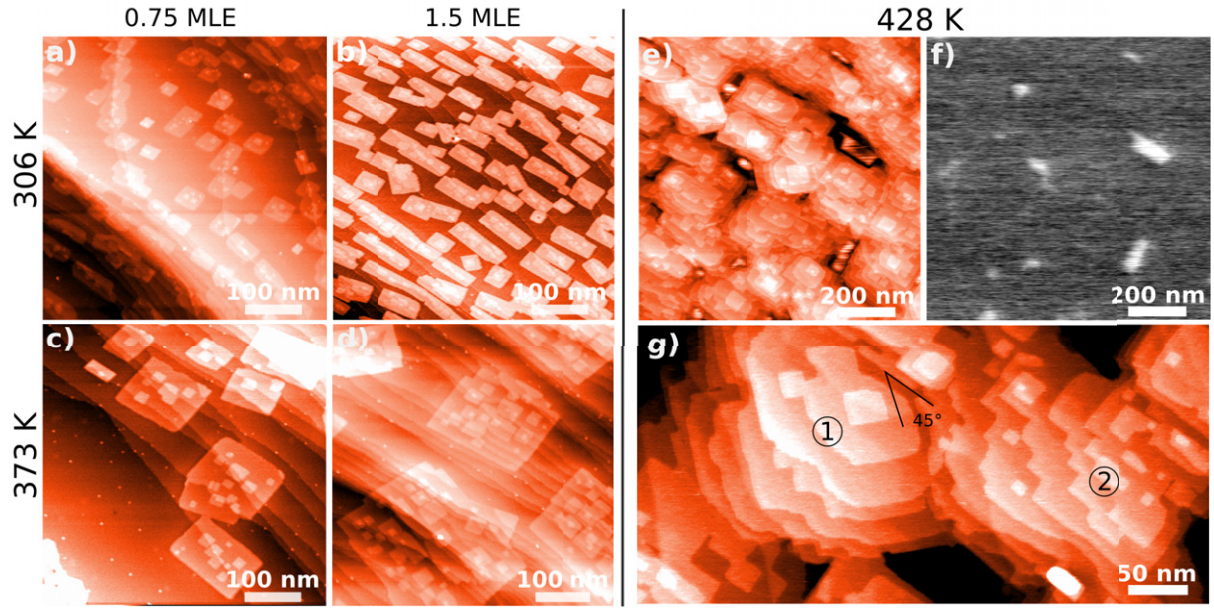

Figure 3. (a)–(d) nc-AFM images of NaCl thin films grown on Ag(001) at different temperatures (rows) and with different quantities of NaCl (columns). (e)–(f) Topography (e) and the corresponding KPFM image (f) of a 6 MLE thick NaCl film grown at $T_{Ag} = 428$ K. A flux of 0.4 MLE min^{-1} was used. (g) Higher magnification of the 6 MLE film (topography). Imaging parameters: (a)–(d) 500×500 nm^2, (e), (f) 803×803 nm^2, (g) 495×240 nm^2, speed = 0.5 Hz (2 Hz (b)), $A = 22$ nm (15 nm (b, g)), $f_{ac} = 474$ Hz, $U_{ac} = 150$ mV. Note that Δf (Hz) $= -19$ (a), (c), -31 (d), -5 Hz (e), (f), -8 Hz (g). Image (b) was acquired in STM mode ($U_{bias} = 3$ V, $I = 0.02$ nA).

For $T_{Ag} =$ RT, we observe that some islands are partly 1 ML thick (see above), whereas all islands have a base layer 2 ML thick at $T_{Ag} = 373$ K.

With respect to the ad-islands, an increase in size of the third and fourth NaCl layers can be observed with increasing quantity of NaCl—the films also grow in height. As already mentioned above, a nanometer large region can be seen at the borders of the base islands, which is almost free of ad-islands. The images shown in figures 1(d) and (e) clearly demonstrate that the size of the ad-islands close to the edges of the base islands is much smaller than the ones in the middle of the base islands—a signature that these small ad-islands obtain less directly impinging and diffusing NaCl for their growth since a part of the NaCl is used to build the base island. Furthermore, an analysis of images such as shown in figure 1 shows that the ad-island-free region increases with temperature: at 343 and 373 K, the region has a width of roughly 5–25 nm, whereas at higher temperatures the width of the region is up to 50 nm wide. This means that the diffusion length of impinging and landing NaCl on the base island increases with temperature.

For large quantities of NaCl on Ag(001), the film starts to cover the whole silver surface and the film grows in height. At 6 MLE nominal thickness for instance, the NaCl film covers 98% of the surface (see figure 3(e)). Only at some places is the silver surface still visible, which can

Table 2. Properties of the NaCl thin films as a function of substrate temperature T_{Ag} and NaCl coverage during growth. The first two columns correspond to depositions at RT (0.75 and 1.5 MLE), whereas the last two columns show values for the films grown at 373 K. The parameters A_{base}, a, ρ and C denote the average base island size ($\times 10^{-11}$ cm^2), the side length a in nm of the island assuming a square shape ($a = b$), the island density ($\times 10^8$ islands cm^{-2}) and the percentage of Ag(001) surface covered by NaCl islands (%).

T_{Ag}	306 K		373 K	
	0.75 MLE	1.5 MLE	0.75 MLE	1.5 MLE
A_{base}	1.3 ± 0.1	1.7 ± 0.2	7.5 ± 1.0	28 ± 6
a ($a = b$)	36	41	87	169
ρ	230 ± 20	252 ± 20	35 ± 2	16 ± 2
C	29 ± 2	44 ± 2	28 ± 2	47 ± 3
$A \times \rho$	0.299	0.428	0.210	0.456

be best seen by the Kelvin image in figure 3(f) (silver: bright regions). Because the underlying silver steps are difficult to find, the height of the film can only be roughly estimated: at some local positions on the surface we estimate a film thickness of up to 9 ML.

The film grows in a three-dimensional (3D) fashion as can be seen in figures 3(e) and (g). The orientation of the steps can vary from hill to hill as exemplified by the two hills, 1 and 2, in figure 3(g). This orientation stems from the 45° and 0° base islands, which exist at low coverages (figure 1).

4. Kelvin probe force microscopy measurements

As the topography images were obtained, the Kelvin modulation was active such that Kelvin images could be simultaneously recorded. Representative Kelvin images are displayed in figure 1 directly below the corresponding topography images. They reflect variations of the surface WF where a dark contrast belongs to a lower WF and vice versa, a bright contrast to a higher WF. All the films which we have prepared for this study show that the NaCl islands appear always with a dark contrast with respect to silver (bright), which means that the system WF is reduced by NaCl for all T_{Ag}.

For a quantitative determination of the WF change, we considered only saturated values for U_{CPD} in profiles of each Kelvin image, at representative Ag and NaCl sites (figure 1). As can be seen in table 1, values taken from histograms yield too small values, especially for small NaCl islands at RT, which is due to the convolution of the surface with the tip (see also figures 2(a) and (b)). Only in the case of large islands do values taken from profiles and histograms agree with each other (see the discussion in [29, 33]).

All thin NaCl films show that the WF difference between Ag(001) and NaCl/Ag(001) is $\Delta\phi = \phi_{Ag} - \phi_{NaCl/Ag} = 0.69 \pm 0.03$ eV. This value is observed from the first NaCl monolayer and the WF between Ag and NaCl/Ag remains constant even if the island thickness varies as can be clearly observed, e.g., in all Kelvin images in figure 1—the dark contrast is uniform over the entire NaCl islands, whereas multiple layer growth is observed in the corresponding topographic images.

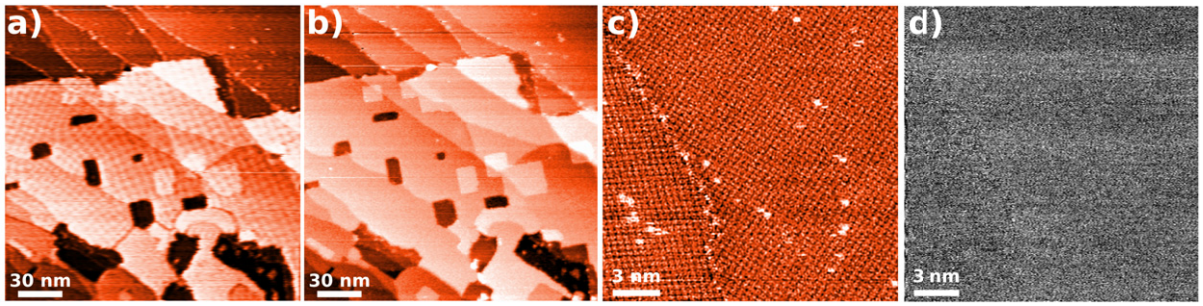

Figure 4. (a) STM image of a NaCl thin film grown on Ag(001) ($U_{bias} = +3.0$ V, $I = 0.02$ nA). A moiré pattern can be observed on the island. (b) nc-AFM image of the same area ($\Delta f = -7$ Hz) in which no moiré pattern can be seen. (c) nc-AFM topography image with atomic resolution of the same islands rotated 45° with respect to each other ($\Delta f = -11$ Hz). (d) Corresponding KPFM image (80 mV rms noise). No local variation of the WF is observed. Imaging parameters: (a), (b) 200×200 nm^2, (c), (d) 30×30 nm^2. For all: speed= 0.5 Hz (2 Hz (a)), $A = 22$ nm. For (b)–(d): $f_{ac} = 474$ Hz, $U_{ac} = 150$ mV.

The WF change of ∼700 meV and its independence of the film thickness are in perfect agreement with predictions from theory for the first 1–3 layers (700 meV [24]). Our value can be compared with films on other metal substrates such as copper and gold [31, 33]. A very important question is if the thickness independence is also valid for thicker films. As exemplified by the KPFM measurement in figures 3(e) and (f), we found that the WF does not change with increasing film thickness—no contrast variations can be seen among different thick layers, and for 6 MLE thick layers (5–9 ML) the WF change remains $\Delta\phi = 0.61 \pm 0.05$ eV. The latter value for the WF change is about 100 mV smaller than the value mentioned above, which is due to a convolution effect—the silver regions are small (20–50 nm) and comparable to the tip apex size.

As also recently discovered on MgO/Mo(001) [28], Pivetta *et al* [22] observed a moiré pattern with STM on the 45° NaCl islands at, e.g., a bias voltage of +3.0 V corresponding to the ground state of the image potential spectrum. They assign this to a strong local modulation of the WF and/or a possible Stark effect [22, 23] and found values for the amplitude of the WF changes of 0.15 V (experiment) and 0.38 eV (theory) [22].

In order to verify possible lateral WF variations, we have made STM and nc-AFM/KPFM measurements. The measurements were made in three steps: first, representative 45° NaCl islands (2 ML thick) were imaged by STM with the AFM tip oscillating at its resonance frequency (figure 4(a)). The tip was then retracted to switch from the STM mode to the nc-AFM mode with the tip oscillation still active. The tip was then gently approached to the surface to avoid any tip changes, which would influence the imaging. The same 45° NaCl islands were then imaged several times in the nc-AFM and KPFM mode (figure 4(b)). We could obtain topography and Kelvin images with high magnification, where the atomic contrast in the topography image is visible (figures 4(c) and (d)). At the end of the image series, the tip was retracted a second time to switch back to the STM mode, to repeat the initial STM measurement.

The first and last STM images of the whole series could reproduce the moiré pattern only on the islands rotated by 45° (figure 4(a)). The moiré pattern has a periodicity of ∼7.8 nm, whereas

the corrugation observed is about 0.07 nm at $U_{bias} = +3.0$ V. The mean value of the periodicity corresponds to the ad-layer–substrate lattice mismatch of 2.1%. However, the periodicity may slightly change from region to region on the 2 ML thick island, which is due to small deviations of the 45° island rotation with respect to the Ag crystal lattice as discussed above and reported earlier [22, 37]. When imaging these islands in nc-AFM with the Kelvin modulation active, neither moiré nor any contrast variation in all our Kelvin images could be observed on the same scale (figure 4(b)). Even when the islands were imaged with atomic resolution in the topography image (figure 4(c)), no contrast could be found in the corresponding Kelvin image (figure 4(d)).

In most cases nc-AFM images with atomic resolution show perfectly atomic flat terraces and no height variations (see, e.g., figure 4(c)). However, in very rare cases we do observe a moiré contrast (not shown) with an extremely faint corrugation of <0.04 nm. Since such a contrast is observed only occasionally it can be assumed that the contrast strongly depends on the chemical nature of the tip. In any case, no contrast in Kelvin images can be seen even in these situations.

5. Discussion

5.1. Film growth

With respect to the growth of the NaCl film on silver (001) the main results can be summarized as follows.

- There is a net increase in island size as T_{Ag} increases. Inversely, the island density decreases. Energies of 0.30 and 0.66 eV were deduced from the density versus T_{Ag} studies.
- The initial nucleation takes place at the steps of the silver surface.
- 1 and 2 ML thick NaCl islands are formed at $T_{Ag} = \mathrm{RT}$ and low coverages. On these islands, the second layer grows from the edges forming a rim or are pinned at the underlying Ag step.
- At elevated temperatures ($T_{Ag} > 343$ K), a large and 2 ML thick base island is always formed.
- At elevated temperatures ($T_{Ag} > 343$ K), ad-islands are never located at the edges of the 2 ML base island. A 10–50 nm large region free of ad-islands can be found on the edges of the base islands.
- Very thick films grow in a 3D fashion, exhibiting 0° and 45° rotated steps and terraces up to 50 nm wide.

Quadrupole mass spectrometry measurements have shown that when a NaCl crystal is vacuum annealed in a Knudsen cell at elevated temperatures, single NaCl molecules evaporate from the crystal in the form of monomers (NaCl) and dimers (Na_2Cl_2) with a monomer/dimer ratio close to 10 [46, 47]—such molecules are therefore the building blocks of the films we describe here. Initially, the molecules land on the surface, nucleate at the steps of silver and act as anchoring sites for other diffusing molecules. Because almost all islands nucleate at the Ag steps, even at $T_{Ag} = 306$ K, it can be anticipated that the mean diffusion length of NaCl molecules on silver (001) must be quite large. The diffusion length is at least comparable to the mean distance between the steps of the silver surface (mean distance: 36 ± 11 nm) and larger than the diffusion length of MgO [45]. An important finding is that the island shape is anisotropic at

$T_{Ag} = 343$ K (figure 1(b))—the islands grow along the steps. This dramatically changes at all higher temperatures, where the islands are close to square shaped and cover many silver steps. From this we conclude that a large part of NaCl molecules overcome the silver steps at temperatures higher than $T_{Ag} \approx 370$ K; however, nucleation of islands still takes place at the steps of silver.

Several models based on rate equations describe the growth of thin films or clusters on a substrate, which has been extensively discussed [48–50] and reviewed [51, 52] in the literature. Such models allow extracting the adsorption and diffusion energy from the density versus temperature curves at low (complete condensation) and high temperatures (incomplete condensation) [51]. However, such a description is quite complicated [53] if the growth is influenced by defects on the surface as is the case here: a defect-driven growth takes place for NaCl on silver since all NaCl islands are located at the steps at almost all temperatures. This clearly contrasts with the situation of MgO thin films on the same substrate: many MgO islands can be found on the atomically flat terraces of silver at almost all temperatures ($373 < T_{Ag} < 673$ K) [45]. For the latter film, two branches were observed in the density versus temperature curves ($\Delta E_1 = 0.23$ eV and $\Delta E_2 = 0.8$ eV [45]), which can be assigned to the low and high temperature cases of an MgO island growth. In contrast, the origin of the energies obtained on NaCl films ($\Delta E_1 = 0.30$ eV for small T_{Ag} and $\Delta E_2 = 0.66$ eV for high T_{Ag}) remains unknown so far. We merely address the change of the slope (from ΔE_1 to ΔE_2) partially to the phenomena where NaCl molecules can overpass the silver steps at higher temperatures ($373\,\text{K} < T_{Ag}$). This is in accordance with the shape of the islands at various temperatures. As mentioned above, at low temperatures the islands are elongated in the direction parallel to the Ag steps. This anisotropy disappears for higher temperatures and the shape of the islands becomes 'square-like'. In the latter case, the limited diffusion of NaCl molecules at Ag steps is lifted and the molecules cover a distance which is larger than the mean Ag–Ag step distance.

In the following, the rim on the 1 ML thick base islands and the ad-island-free region at the borders of the 2 ML base islands are discussed. Our and other works [22, 37] show that at low temperatures ($T_{Ag} \leqslant$ RT) the molecules build 1 ML thick islands first. A part of these base islands exhibit a rim at their edges with their center still 1 ML thick (figure 5(a), left),[3] which is not observed on 2 ML islands (see below). This points to a significant difference between the first and second monolayers of NaCl on silver. STM [22] and SPA-LEED [37] measurements revealed a contraction of the NaCl unit cell by about 0.9%, which changes as a function of film thickness such that the bulk value of the unit cell is reached at a thickness of 10 ML and more [37]. Recent numerical calculations considered the strain that appears in 1 and 2 ML thick MgO islands supported on a metal surface (weak interaction) [26]. The calculations show that the strain is quite local and pronounced for 1 ML thick islands but less for 2 ML thick islands—a phenomenon which may also appear for NaCl/Ag(001). Despite the lack of evidence, we tentatively address our observations to the differences in the lattice strain for 1 and 2 ML thick islands. Due to strain in the 1 ML thick islands, an Ehrlich–Schwoebel barrier could be present at the edges of the islands as shown in figure 5(b) (left): when depositing NaCl, a small part of the molecules impinges on already existing 1 ML thick islands and diffuses to the edges. The latter are energetically more favorable for adsorption of the molecules with respect to the center of the island so that a rim is built at the edges of the base islands. However, the

[3] www.blender.org (2012).

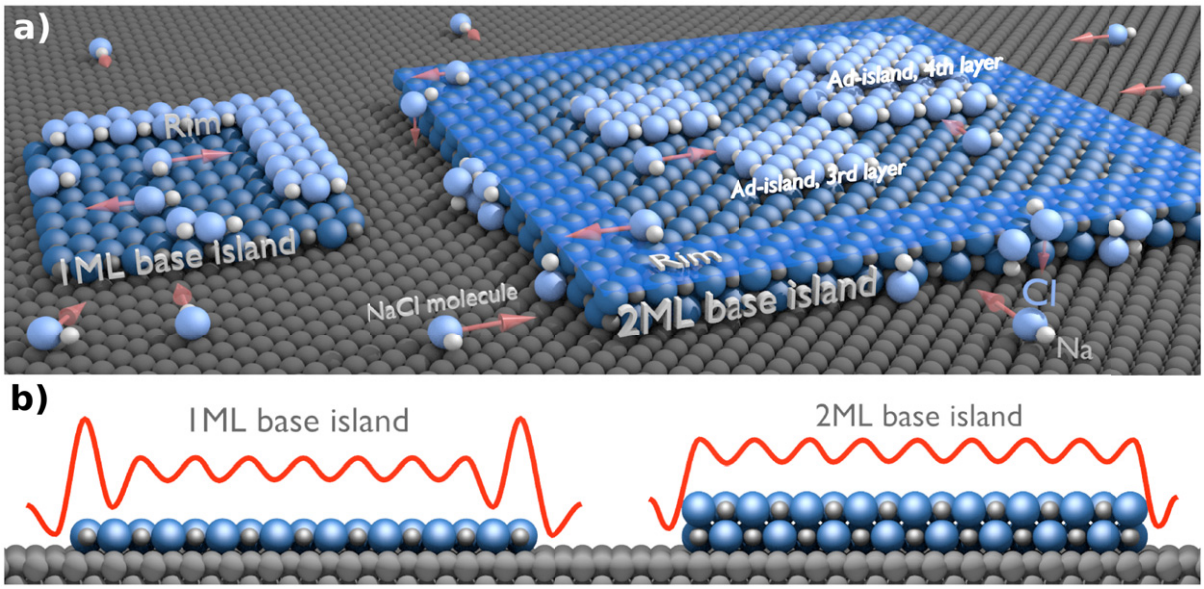

Figure 5. (a) Model for the NaCl island growth on Ag(001). Impinging NaCl molecules on the silver substrate diffuse and build the 1 ML (left) and 2 ML base islands (right) at RT or higher temperatures, respectively. (b) Energy landscape for NaCl molecules on the 1 and 2 ML base islands. For 1 ML islands an Ehrlich–Schwoebel barrier leads to the formation of a rim at the edges (left). This barrier does not exist for the 2 ML base island (right). The artwork was produced with Blender (see footnote 3).

NaCl molecules, which diffuse on the silver surface and arrive at the edges of the base island, would not climb on top of the base island because of the high Ehrlich–Schwoebel barrier. We speculate that for 2 ML islands the barrier vanishes possibly due to a smaller strain in the second layer (figure 5(b), right). As will be explained in the following, there is in fact clear experimental evidence that such a barrier does not exist for the second layer.

With respect to elevated temperatures, the island density decreases and the surface area of the base island dramatically increases. Due to the very large surface area of the base islands, a second type of growth plays a fundamental role: NaCl is collected from the incoming NaCl flux on the base islands for building the film. At high temperatures, the molecules are sufficiently mobile on the base island such that they form 1 ML thick ad-islands in the third and fourth layers (figure 5, right). Similar to the situation on the silver surface, the ad-islands get pinned at the underlying Ag step mostly in the middle of the base islands, where they are evenly distributed. The 10–50 nm large, ad-island-free region located at the edges of the base islands gives a clear signature that impinging molecules which land close to the edges of the base island diffuse to the edges and step down such that they contribute to building up the base island. The result is that an ad-island-free area on the base island is created (figure 5, right).

To verify our picture about the film growth a simple model can be done which perfectly explains our observations (see the appendix). The model considers the two different growth contributions: the growth from diffusing molecules on the silver surface for building the base

Table 3. The average experimental (exp) and calculated (calc) sizes of the base islands (A_{base} in 10^{-11} cm^2) and the ad-islands (A_{ad} in %) as a function of the temperature T. The parameter dr is the width of the ad-island-free region in nanometers. Values for d$r = 0$ and d$r \neq 0$ are shown. For the calculations, a flux of $F = 2.6 \times 10^{11}$ NaCl molecules s^{-1} cm^{-2} and a deposition time of $t = 30$ min were used.

T_{Ag}	343 K	373 K	423 K	443 K
dr_{exp}	10	10	30	50
$A_{base,exp}$	4.7 ± 0.3	7.5 ± 1.0	82 ± 10	160 ± 24
$A_{base,calc}$ (d$r = 0$)	4.0	8.6	76	142
$A_{base,calc}$ (d$r \neq 0$)	4.6	9.5	85	161
$A_{ad,exp}$	–	22 ± 7	27	31 ± 5
$A_{ad,calc}$ (d$r = 0$)	60	60	60	60
$A_{ad,calc}$ (d$r \neq 0$)	27	36	36	31

islands and the growth of the ad-islands on top of the latter from directly impinging molecules. The model also respects that a part of the impinging molecules on top of the base island are used to build up the latter. The width dr of the ad-island-free region, the density of islands ρ (see table 1), the flux F and deposition time t are used as an input to calculate the size of the base and ad-islands. The experimental and calculated values are shown in table 3.

For the case when no ad-molecules (molecules landing directly onto NaCl) are used for building up the base island (width d$r = 0$), the surface area of the base island ($A_{base,calc}$ (d$r = 0$)) agrees to some extent with the experimental values ($A_{base,exp}$). However, the coverage of the base islands by the ad-islands ($A_{ad,calc}$ (d$r = 0$)) is always 60%, which is twice as large as the mean experimental value ($A_{ad,exp} \approx 30\%$). Much better agreement is obtained if molecules impinging in a region of dr at the edges of the base islands are taken into account: the calculated sizes for the base islands ($A_{base,calc}$ (d$r \neq 0$)) agree much better with the experimental values ($A_{base,exp}$). More importantly, the coverage of the base islands by the ad-islands ($A_{ad,calc}$ (d$r \neq 0$)) is in very good agreement with the experimental values ($A_{ad,exp}$), a mean value of about 30% is obtained. Note that, due to the experimental AFM observations and the latter perfect match, a net upward movement of molecules onto the 2 ML base island can be excluded.

For thicker films, the fourth layer and successive layers will start growing. Important is the influence of the silver surface and its atomic high steps, which considerably modify the flatness of especially very large islands with side lengths of several hundreds of nm. Moreover, a coalescence of islands can be expected at high coverages. Our LEED measurements have shown that each island exhibits slightly different orientations with respect to the silver lattice (see also LEED and SPA-LEED work in [39] and [37], respectively), which means that dislocations or grain boundaries are created during the coalescence of islands. The latter defects destroy an overall perfect atomic lattice of thick films and are potential sites for following island growth. The coalescence of two differently oriented NaCl islands can be best observed by NaCl steps on thick films: when a 0° and a 45° island in the sub-monolayer regime coalesce they guide the growth for a thick NaCl film. The result is that the thick film exhibits NaCl steps, which are rotated with respect to each other by ∼45° (figure 3(g)).

5.2. Work function measurements

A large reduction of the silver WF of $\Delta\phi = 0.69 \pm 0.03$ eV is obtained above the NaCl islands. This value is obtained for the first monolayer of NaCl, and no further variation is observed as the NaCl film thickness increases. Although our values for the WF change are lower than the ones obtained by STM ($\Delta\phi = 1.3$ eV) [22, 23], they are in perfect agreement with values stemming from recent theoretical calculations ($\Delta\phi = 0.70$ eV) [24], which address the WF change to an electrostatic compression effect. Furthermore, the latter work predicts no thickness dependence, which is in excellent agreement with our experimental data. Our KPFM data even show that the WF does not change when the silver surface is covered by 6 ML NaCl—the WF change is determined by the interfacial layer for all thicknesses.

With respect to possible lateral variations of the WF on 45° islands, no Kelvin contrast within any of these islands could be observed, although a clear moiré contrast on the same islands was measured in STM images. We rule out the possible explanation that the tip apex was too far away from the surface since KPFM has been obtained simultaneously with the atomic resolution in the detuning image. The latter is a clear sign that the tip was close enough for detecting WF variations in the range of 100 mV at the nanometer length scale.

The precise nature of the moiré pattern observed under STM experiments remains unknown so far. However, we rule out the predicted variations of 150 or 380 mV [12], which should have been visible in our KPFM images otherwise. KPFM is sensitive to any kind of change in the electrostatics of the surface so that a partial charge variation induced by any kind of electronic effect should be visible. We assume that the Moiré pattern is probably a pure electronic phenomenon in STM at elevated voltages. Note that KPFM always minimizes electrostatic forces between the tip and the surface and that the measured absolute Kelvin voltages (U_{CPD}) for all measurements shown here are always much lower than 1 V and far away from any of the ground states of the image potentials.

6. Conclusion

The NaCl thin-film growth on silver (001) as a function of temperature and NaCl quantity and the WF of this thin-film system are described and discussed in this paper. As the substrate temperature increases during deposition of NaCl in the sub-monolayer regime, the island size increases with a decrease in density. Islands with sizes of up to 400 nm are formed at highest temperatures ($T_{\mathrm{Ag}} = 443$ K). At high temperatures ($T_{\mathrm{Ag}} >$ RT), 2 ML thick base islands are always formed with some ad-islands in the third and fourth layers on top. The ad-islands are always located in the middle of the base islands, whereas a rim up to 50 nm wide at the edges of the base islands is ad-island-free. These observations show that impinging NaCl molecules on 2 ML thick base islands are used to build not only the ad-islands but also the base islands, which is verified by a simple model.

The film covers the whole silver surface from a nominal thickness of 6 MLE and exhibits a 3D growth. Because the NaCl islands slightly differ in their orientation with respect to the silver lattice in the sub-monolayer regime, dislocations or grain boundaries are created due to island coalescence during the growth of thick films. This can be indirectly seen by NaCl steps rotated with respect to each other by 45°, which belong to former 0° and 45° islands in the sub-monolayer regime.

In perfect agreement with predictions from theory [24], KPFM yields a reduction of the silver WF by NaCl of $\Delta\phi = \phi_{\mathrm{Ag}} - \phi_{\mathrm{NaCl}} = 0.69 \pm 0.03$ eV, which is obtained as early as the first monolayer of NaCl, with no further changes for thicker layers (6 MLE nominal thickness). None of the moiré patterns observed in STM were observed on any of the 45° NaCl islands in KPFM, which rules out that the WF varies laterally in the range of 100 meV and more. The origin of the moiré observed in STM is probably a purely electronic phenomenon. However, its origin remains unknown so far.

Acknowledgments

We gratefully acknowledge the French Agency for Research (Agence Nationale pour la Recherche) for financial support through the P3N program (the project MISS). CB also acknowledges support from the European Science Foundation by the FANAS project NOMCIS and the COST Action CM1104. Stimulating discussions with W D Schneider, S Gauthier, M Hanbücken, I Beinik, J Goniakowski and C Noguera are gratefully acknowledged.

Appendix

For describing the NaCl film growth, we use the model of Sigsbee [48] and Stowell [54], which has been extended by Kashchiev [50]. In this model, it is assumed that the film is composed of disc-shaped islands evenly distributed on the substrate and competing amongst each other for capturing incoming molecules that build the islands. In our case, we only consider single NaCl molecules for simplicity. Furthermore, the model assumes that the islands are built only by molecules diffusing on the surface of the substrate and that the diffusion length of the molecules is larger than the mean island–island distance, which is the case for NaCl molecules on Ag(001). The surface area A_{base} of a growing island is then described by the following equation:

$$A_{\mathrm{base}} = \frac{F}{N_0\, n_{\mathrm{s}}} \times t = C_1\, t. \tag{A.1}$$

The parameters F, N_0, n_{s} and t denote the incoming flux (NaCl molecules $\mathrm{cm}^{-2}\,\mathrm{s}^{-1}$), the density of NaCl adsorption sites in the layer (sites cm^{-2}), the density of NaCl islands on silver (islands cm^{-2}) and the deposition time. Assuming a crystalline base island, the density of adsorption sites in the base island is given by $N_0 = 4/a_{\mathrm{NaCl}}^2$, where a_{NaCl} is the size of the unit cell of NaCl. Note that the base layer is 2 ML thick, so that four NaCl molecules in the vertical position can be found in the area of a_{NaCl}^2.

When the base island increases in size with time, it collects an increasing number of directly impinging NaCl molecules. The flux J of impinging NaCl molecules on the base island is simply given by

$$J = A_{\mathrm{base}}\, F = C_1\, t\, F.$$

The flux J is measured in units of the number of molecules s^{-1}. Assuming that only 1 ML high and crystalline ad-islands are formed on the top of the base island, the overall surface area of the ad-islands is simply

$$A_{\mathrm{ad}} = J\, A_{\mathrm{NaCl}}\, t = C_1\, F\, A_{\mathrm{NaCl}}\, t^2 = \frac{F^2\, A_{\mathrm{NaCl}}}{N_0\, n_{\mathrm{s}}} \times t^2, \tag{A.2}$$

where A_{NaCl} is the surface area of a single NaCl molecule in horizontal orientation ($A_{\mathrm{NaCl}} = \frac{1}{2}a^2_{\mathrm{NaCl}}$).

The AFM experiments clearly show that part of the impinging NaCl molecules on the base islands is used to build the latter islands. We consider now the total number of NaCl molecules in one complete NaCl island (base island + ad-island), which can be expressed by the surface area: $2 \times A_{\mathrm{base}} + A_{\mathrm{ad}}$. Note that the factor of 2 is due to the base island, which is 2 ML thick and which contains twice as many molecules in comparison to a 1 ML thick ad-island of the same projected area. We expand the latter equation as follows:

$$2 \times A_{\mathrm{base}} + A_{\mathrm{ad}} = 2 \times A_{\mathrm{base}} + A_{\mathrm{ad}}\, f + A_{\mathrm{ad}} - A_{\mathrm{ad}}\, f.$$

The first part of the right-hand side in the latter equation can now be ascribed as the new surface area of the base island A'_{base}, whose surface area is increased by $A_{\mathrm{ad}}\, f$ of impinging NaCl molecules. The second part is the new surface area of the ad-island A'_{ad}, whose surface area is reduced by $A_{\mathrm{ad}}\, f$:

$$A'_{\mathrm{base}} = 2 \times A_{\mathrm{base}} + A_{\mathrm{ad}}\, f, \tag{A.3}$$

$$A'_{\mathrm{ad}} = A_{\mathrm{ad}} - A_{\mathrm{ad}}\, f. \tag{A.4}$$

The parameter f is the percentage (between 0 and 1) of impinging NaCl molecules used for building the base island. If we assume that such molecules are collected in only a small region with constant thickness Δr at the edge of the circular base island (radius $r = \sqrt{\frac{F}{\pi\, N_0\, n_s}\, t}$), the relative percentage is given by

$$f = \frac{\pi\, r^2 - \pi\, (r - \Delta r)^2}{\pi\, r^2}. \tag{A.5}$$

With equations (A.1)–(A.5), the surface area of the base island (A'_{base}) and of the ad-islands (A'_{ad}) can be calculated with known values from the experiments for the flux F of incoming NaCl molecules, the island density n_{s}, the deposition time t and the width of the collecting area at the edges of the NaCl base island Δr.

References

[1] Parkin S S P, Kaiser C, Panchula A, Rice P M, Hughes B, Samant M and Yang S-H 2004 *Nature Mater.* **3** 862
[2] Yuasa S, Nagahama T, Fukushima A, Suzuki Y and Ando K 2004 *Nature Mater.* **3** 868
[3] Heiz U and Landman U 2007 *Nanocatalysis* (Berlin: Springer)
[4] Freund H J and Pacchioni G 2008 *Chem. Soc. Rev.* **37** 2224
[5] Cañas-Ventura M E, Xiao W, Ruffieux P, Rieger R, Müllen K, Brune H and Fasel R 2009 *Surf. Sci.* **603** 2294
[6] Sun X and Silly F 2010 *Appl. Surf. Sci.* **256** 2228
[7] Abel M, Clair S, Ourdjini O, Mossoyan M and Porte L 2011 *J. Am. Chem. Soc.* **133** 1203
[8] Bombis Ch, Ample F, Lafferentz L, Yu H, Hecht S, Joachim Ch and Grill L 2009 *Angew. Chem., Int. Ed. Engl.* **48** 9966
[9] Filleter T, Paul W and Bennewitz R 2008 *Phys. Rev.* B **77** 035430
[10] Gross L, Mohn F, Moll N, Liljeroth P and Meyer G 2009 *Science* **325** 1110

[11] Guillermet O, Gauthier S, Joachim C, De Mendoza P, Lauterbach T and Echavarren A 2011 *Chem. Phys. Lett.* **511** 482
[12] Ćavar E, Blüm M-Ch, Pivetta M, Patthey F, Chergui M and Schneider W-D 2005 *Phys. Rev. Lett.* **95** 196102
[13] Repp J and Meyer G 2006 *Appl. Phys.* A **85** 399
[14] Liljeroth P, Repp J and Meyer G 2007 *Science* **317** 1203
[15] Gross L, Mohn F, Liljeroth P, Repp J, Giessibl F J and Meyer G 2009 *Science* **324** 1428
[16] Leoni Th, Guillermet O, Walch H, Langlais V, Scheuermann A, Bonvoisin J and Gauthier S 2011 *Phys. Rev. Lett.* **106** 216103
[17] Fölsch S, Helms A, Zophel S, Repp J, Meyer G and Rieder K-H 2000 *Phys. Rev. Lett.* **84** 123
[18] Fölsch S, Helms A, Riemann A, Repp J, Meyer G and Rieder K-H 2002 *Surf. Sci.* **497** 113
[19] Bombis Ch, Ample F, Mielke J, Mannsberger M, Villagómez C J, Roth Ch, Joachim C and Grill L 2010 *Phys. Rev. Lett.* **104** 185502
[20] Olsson F E and Persson M 2003 *Surf. Sci.* **540** 172
[21] Butti G, Trioni M I and Ishida H 2004 *Phys. Rev.* B **70** 195425
[22] Pivetta M, Patthey F, Stengel M, Baldereschi A and Schneider W D 2005 *Phys. Rev.* B **72** 115404
[23] Ploigt H C, Brun C, Pivetta M, Patthey F and Schneider W D 2007 *Phys. Rev.* B **76** 195404
[24] Prada S, Martinez U and Pacchioni G 2008 *Phys. Rev.* B **78** 235423
[25] Harding C, Habibpour V, Kunz S, Farnbacher A N S, Heiz U, Yoon B and Landman U 2009 *J. Am. Chem. Soc.* **131** 538
[26] Noguera C, Godet J and Goniakowski J 2010 *Phys. Rev.* B **81** 155409
[27] Guo Q, Qin Zh Liu C, Zang K, Yu Y and Cao G 2010 *Surf. Sci.* **604** 1820
[28] Benedetti S, Stavale F, Valeri S, Noguera C, Freund H-J, Goniakowski J and Nilius N 2012 *Adv. Funct. Mater.* **604** at press doi:10.1002/adfm.201201502
[29] Bieletzki M, Hynninen T, Soini T M, Pivetta M, Henry C R, Foster A S, Esch F, Barth C and Heiz U 2010 *Phys. Chem. Chem. Phys.* **12** 3203
[30] Sterrer M, Risse T, Pozzoni U M, Giordano L, Heyde M, Rust H P, Pacchioni G and Freund H-J 2007 *Phys. Rev. Lett.* **98** 096107
[31] Loppacher C, Zerweck U and Eng L M 2004 *Nanotechnology* **15** 9
[32] Krok F, Sajewicz K, Konior J, Goryl M, Piatkowski P and Szymonski M 2008 *Phys. Rev.* B **77** 235427
[33] Glatzel T, Zimmerli L, Koch S, Such B, Kawai S and Meyer E 2009 *Nanotechnology* **20** 264016
[34] Nonnenmacher M, O'Boyle M P and Wickramasinghe H K 1991 *Appl. Phys. Lett.* **58** 2921
[35] Kitamura S, Suzuki K and Iwatsuki M 1999 *Appl. Surf. Sci.* **140** 265
[36] Barth C, Foster A S, Henry C R and Shluger A L 2011 *Adv. Mater.* **23** 477
[37] Le Moal E, Müller M, Bauer O and Sokolowski M 2009 *Surf. Sci.* **603** 2434
[38] Kiguchi M, Entani S, Saiki K, Inoue H and Koma A 2002 *Phys. Rev.* B **66** 155424
[39] Kramer J, Tegenkamp C and Pfnür H 2003 *J. Phys.: Condens. Matter* **15** 6473
[40] Ramoino L, von Arx M, Schintke S, Baratoff A, Güntherodt H-J and Jung T A 2006 *Chem. Phys. Lett.* **417** 22
[41] Barth C, Claeys C and Henry C R 2005 *Rev. Sci. Instrum.* **76** 083907
[42] Barth C and Henry C R 2006 *Nanotechnology* **17** S155
[43] West A R 1985 *Solid State Chemistry and its Applications* (New York: Wiley)
[44] Ashcroft N W and Mermin N D 1976 *Solid State Physics* (Pacific Grove, CA: Brooks Cole)
[45] Ouvrard A, Niebauer J, Ghalgaoui A, Barth C, Henry C R and Bourguignon B 2011 *J. Phys. Chem.* C **115** 8034
[46] Berkowitz J and Chupka W A 1958 *J. Chem. Phys.* **29** 653
[47] Lester J E and Somorjai G A 1968 *J. Chem. Phys.* **49** 2940

[48] Sigsbee R A 1971 *J. Appl. Phys.* **42** 3904
[49] Robinson V N E and Robins J L 1974 *Thin Solid Films* **20** 155
[50] Kashchiev D 1978 *Thin Solid Films* **55** 399
[51] Venables J A, Spiller G D T and Hanbucken M 1984 *Rep. Prog. Phys.* **47** 399
[52] Henry C R 1998 *Cryst. Res. Technol.* **33** 1119
[53] Venables J A 1994 *Surf. Sci.* **299** 798
[54] Stowell M J 1972 *Phil. Mag.* **26** 349